Eur. Phys. J. B (2019) 92: 114
https://doi.org/10.1140/epjb/e2019-90642-8

THE EUROPEAN PHYSICAL JOURNAL B

Regular Article

Dynamics of an inhomogeneously broadened passively mode-locked laser*

Alexander Pimenov[1] and Andrei G. Vladimirov[1,2,a]

[1] Weierstrass Institute, Mohrenstr. 39, 10117 Berlin, Germany
[2] Lobachevsky State University of Nizhni Novgorod, pr. Gagarina 23, Nizhni Novgorod 603950, Russia

Received 2 November 2018 / Received in final form 31 January 2019
Published online 22 May 2019

Abstract. We study theoretically the effect of inhomogeneous broadening of the gain and absorption lines on the dynamics of a passively mode-locked laser. Using numerical simulations of travelling wave equations, we demonstrate the formation of an instability of mode-locking regime and suppression of Q-switching in a laser with large inhomogeneous broadening. Moreover, we derive simplified delay-differential equation model for a mode-locked laser with inhomogeneously broadened gain and absorption lines and perform numerical bifurcation analysis of this model.

1 Introduction

Passively mode-locked lasers generate short optical pulses used in numerous scientific, technological, and industrial applications. In particular, monolithic semiconductor lasers are compact sources of picosecond and subpicosecond pulses with high repetition rates suitable for application in telecommunication networks [1]. Recent experimental and theoretical investigations have demonstrated important advantages of new generations of quantum dot and quantum dash semiconductor lasers over conventional quantum-well semiconductor devices: low threshold current, low pulse chirp, reduced temperature sensitivity, high stability to noise and external feedback, etc. [2,3]. One of the important features of these lasers that plays a major role in determining various laser characteristics is the inhomogeneous broadening of the gain spectrum due to nonuniformity of the ensemble of quantum dots with respect to their size, shape, and composition [2]. In particular, it was demonstrated that in quantum dot lasers under the bias conditions the inhomogeneous broadening width at half-maximum (from 21 meV to 50 meV) is larger than homogeneous broadening width (19 meV) [4].

The effect of inhomogeneous broadening on single-mode [5–11], multi-longitudinal [12–19] and multitransverse [20,21] mode laser instabilities has been a subject of intense studies during the past decades. In particular, it was shown that inhomogeneous broadening can reduce the so-called second laser threshold as well as the threshold of the multimode Risken-Nummendal-Graham-Haken instability leading to a self-pulsing behaviour. This is in agreement with the well known fact [22] that inhomogeneous broadening of the gain line leads to a reduction of mode competition and, hence, can facilitate multimode operation. On the other hand, a suggestion that due to reduced mode-competition ultrashort-pulse formation may be more easily achievable in inhomogeneously broadened lasers than in corresponding homogeneous systems, were shown to be in contradiction with the experimental data [23]. This can be understood by taking into account that increasing inhomogeneous broadening introduces additional incoherence into mode interaction and, therefore, can reduce the intervals where self-pulsing is observed [19].

While the dynamics of inhomogeneously broadened CW lasers has been already extensively investigated, the influence of inhomogeneous broadening on the characteristics of passively mode-locked lasers still remains largely unexplored theoretically. In order to fill this gap in this work we study numerically the dynamics of a passively mode-locked laser with inhomogeneously broadened gain and absorber lines. We consider traveling wave equations (TWEs) for the electric field envelopes of the counter-propagating waves coupled to the equations for polarisations and population differences of the two-level atoms emitting at different central frequencies [21]. We integrate the resulting integro-differential equations numerically with the help of an efficient spectral method with Hermite-Gaussian functions taken as the basis. To this end, similarly to Graham and Cho [7], we derive an infinite chain of equations for the macroscopic variables, truncate this chain, and solve the truncated equations numerically. Unlike the analytical approach of

* Contribution to the Topical Issue "Non-Linear and Complex Dynamics in Semiconductors and Related Materials", edited by Kathy Lüdge.

[a] e-mail: vladimir@wias-berlin.de

Graham and Cho [7], our numerical techniques allow us to perform the truncation at much higher orders and, therefore, to achieve higher precision. Basing on our simulations we demonstrate that for moderate values of the inhomogeneous broadening linewidth the mode-locking characteristics can be improved due to suppression of the Q-switching instability. On the other hand, large inhomogeneous broadening linewidths lead eventually to a degradation of the mode-locking regime.

Finally, by assuming unidirectional propagation of the electrical field in the ring cavity and using the approach proposed in [24–26], we derive a simplified delay-differential equation (DDE) model of a mode-locked laser with inhomogeneously broadened gain and absorption lines. This model provides a good qualitative description of the nonlinear dynamical regimes in a laser by taking into consideration zero and first moments of medium polarisation [7,10]. We perform numerical bifurcation analysis of the DDE model and demonstrate qualitative agreement with the TWE model. We show that an instability of the mode-locking regime develops when the inhomogeneous broadening width of the gain line exceeds a certain threshold. On the other hand, suppression of Q-switching instability of the fundamental mode-locked regime can be achieved at sufficiently large inhomogeneous broadening linewidth of the saturable absorber.

2 Model equations

2.1 Travelling wave model

We consider non-dimensional form of the TWE model describing space-time evolution of the amplitudes $E^{\pm}(t,z)$ of the two counter-propagating waves, corresponding polarisations $P^{\pm} = P^{\pm}(\bar{\omega},t,z)$, and population difference $N = N(\bar{\omega},t,z)$ of the two-level inhomogeneously broadened medium. These equations are obtained from the two-level semiclassical Maxwell-Bloch equations under standard mean-field, effective-index, and slowly varying envelope approximations [21]

$$\frac{\partial E^{\pm}}{\partial t} \pm \frac{\partial E^{\pm}}{\partial z} = -\frac{\beta}{2}E^{\pm} + \int_{-\infty}^{\infty} P^{\pm}\bar{f}(\bar{\omega})d\bar{\omega}, \tag{1}$$

$$\frac{\partial P^{\pm}}{\partial t} = (-\Gamma + i\bar{\omega})P^{\pm} + \frac{g}{2}NE^{\pm}, \tag{2}$$

$$\frac{\partial N}{\partial t} = n_0 - \gamma_N N - \Re(P^{+}E^{+*} + P^{-}E^{-*}). \tag{3}$$

Here β describes internal linear losses in the intracavity medium, g is the differential gain parameter, Γ and γ_N are the transverse and longitudinal relaxation rates, respectively, and $n_0 = n_0(z)$ is the linear gain/loss parameter. The normalised spectral distribution $\bar{f}(\bar{\omega})$ is represented by the Gaussian profile

$$\bar{f}(\bar{\omega}) = \frac{1}{\sigma\sqrt{2\pi}}\exp\left(-\frac{(\bar{\omega}-\omega_0)^2}{2\sigma^2}\right), \tag{4}$$

where σ is the width of inhomogeneous broadening at half-maximum, ω_0 is the detuning between the central frequency of the Gaussian distribution (4) and the frequency of one of the cavity modes, which serves as the reference frequency.

2.2 Spectral method

For numerical solution of equations (1)–(4) we use a "spectral" (Galerkin) method. First, we choose Hermite-Gaussian functions

$$\phi_m(\omega) = (m!2^m\sqrt{\pi})^{-1/2}e^{-\omega^2/2}H_m(\omega), \tag{5}$$

where $H_m(\omega)$ is the Hermite polynomial of the order m, as a complete orthonormal basis for the space $L^2(\mathbb{C})$ with the inner product defined by

$$\langle u, v\rangle = \int_{-\infty}^{\infty} uv^* d\omega. \tag{6}$$

After the coordinate change

$$\omega = \frac{\bar{\omega}-\omega_0}{\sqrt{2}\sigma}, \tag{7}$$

the spectral distribution $\bar{f}(\bar{\omega})$ given by equation (4) transforms into $f(\omega) = \phi_0^2$ with $\phi_0 = \pi^{-1/4}e^{-\omega^2/2}$. Therefore, we can rewrite (1) in the form

$$\frac{\partial E^{\pm}}{\partial t} \pm \frac{\partial E^{\pm}}{\partial z} = P_0^{\pm} - \frac{\beta}{2}E^{\pm} \tag{8}$$

with $P_0^{\pm} = \langle P^{\pm}(\omega,t,z)\phi_0(\omega), \phi_0(\omega)\rangle$. Then multiplying equations (2) and (3) with ϕ_0, projecting them onto ϕ_m, taking into account the coordinate change (7), and using the recurrent relations for Hermite polynomials we obtain an infinite hierarchy of equations for the moments $P_m^{\pm}(t,z) = \langle P^{\pm}(\omega,t,z)\phi_0(\omega), \phi_m(\omega)\rangle$ and $N_m(t,z) = \langle N(\omega,t,z)\phi_0(\omega), \phi_m(\omega)\rangle$:

$$\frac{\partial P_m^{\pm}}{\partial t} = (-\Gamma + i\omega_0)P_m^{\pm} + i\sigma(\sqrt{m}P_{m-1}^{\pm} + \sqrt{m+1}P_{m+1}^{\pm}) + \frac{g}{2}N_mE^{\pm}, \tag{9}$$

$$\frac{\partial N_m}{\partial \tau} = n_{0m} - \gamma_N N_m - \Re(E^{+}P_m^{+*} + E^{-}P_m^{-*}), \tag{10}$$

where $P_{-1}^{\pm} \equiv 0$.

In terms of original problem (1)–(3) the first two moments of polarisation and population inversion have the form $P_j^{\pm} = \int_{-\infty}^{\infty}\omega^j P^{\pm}f(\omega)d\omega$ and $N_j = \int_{-\infty}^{\infty}\omega^j N f(\omega)d\omega$ with $j = 0, 1$ and $f(\omega) = \phi_0(\omega)^2$. They are equivalent to the zeroth- and the first-order moments of polarisation $P^{\pm}$ and carrier density N introduced by Graham and Cho [7]. Since $n_{0m} = 0$ for all $m > 0$, only the zeroth-order moment of the population difference is pumped directly, while other moments are excited via a purely imaginary constant in equation (9).

When solving numerically equations (8)–(10) we choose some finite M and truncate them by setting $P^{\pm}_{M+1}=0$. Though there is not much mathematical theory beyond partial integro-differential equations (1)–(3), the finite-dimensional hyperbolic system of PDEs (8)–(10) is well-posed [27]. Using energy estimates for the system (8)–(10) given in [28] one can show that the moments decrease with the number $m>0$, i.e. $|P^{\pm}_m|, |N_m| \le c_k m^{-k}$ with any integer $k>0$ and some constants $c_k>0$ that do not depend on m and M. Therefore, solution of equations (8)–(10) truncated at sufficiently large $m=M$ must be close to that of the same equations truncated at $m=M_1>M$. Or, in other words, this solution must be close to the solution of the non-truncated equations. It is evident from the equation (9) that the speed of decrease of the moments with m depends strongly on the value of σ. In this sense, the chosen approach provides good quantitative approximation with the truncation order $M=1$ for the case of small σ. Moreover, in contrast to more direct approaches where integral in (1) is discretised or replaced with a sum of M atom groups [15,16], quite small number of moments M is often sufficient for adequate description of the laser dynamics as demonstrated in [7] and below. For larger M and higher quantitative accuracy, our approach allows for application of very robust and efficient numerical discretisation schemes similar to those described in [29–32], see Appendix B for more details.

Truncating equations (8)–(10) at $M=1$ and eliminating adiabatically $P^{\pm}_1$ we obtain the following equation for $P^{\pm}_0$:

$$\frac{\partial P^{\pm}_0}{\partial t} = -\left(\Gamma+\frac{\sigma^2}{\Gamma}\right)P^{\pm}_0+\frac{\Gamma}{2}N_0E^{\pm}. \tag{11}$$

Hence, we conclude that for small enough σ the basic effect of inhomogeneous broadening is to increase the homogeneous broadening width Γ by approximately σ^2/Γ.

3 Delay-differential equation model

In this section, we introduce a DDE system to describe an inhomogeneously broadened mode-locked semiconductor laser. First, we derive in Appendix A a DDE model taking into account the polarisation dynamics in two-level active medium. This model can be easily generalised to take into account inhomogeneous broadening. The resulting system of distributed DDEs reads

$$\gamma^{-1}\frac{dA}{dt}+(1-i\omega_0/\gamma)A=\sqrt{\kappa}\left[A(t-\tau)+\langle P_q(\omega_q),f_q(\omega_q)\rangle + \langle P_g(\omega_g),f_g(\omega_g)\rangle\right], \tag{12}$$

$$\frac{dP_q}{dt}=(-\Gamma_q+i\omega_q)P_q+\Gamma_q(e^{-Q/2}-1)A(t-\tau), \tag{13}$$

$$\frac{dP_g}{dt}=-(\Gamma_g-i\omega_g)P_g+\Gamma_g(e^{G/2}-1)[A(t-\tau)+P_q], \tag{14}$$

$$\frac{dQ}{dt}=q_0-\gamma_qQ+s|A(t-\tau)+P_q|^2-s|A(t-\tau)|^2, \tag{15}$$

$$\frac{dG}{dt}=g_0-\gamma_gG+|A(t-\tau)+P_q|^2 -|A(t-\tau)+P_g+P_q|^2, \tag{16}$$

where $A(t)$ is the complex electric field amplitude, $G(t)$ and $Q(t)$ represent saturable gain and absorption introduced by the corresponding laser media. Parameters g_0 and q_0 describe unsaturated gain and absorption, respectively, $\kappa<1$ is the cavity round trip attenuation factor, s is the ratio of the saturation intensities in the gain and absorber media, $\tau=2l$ is the cavity round-trip time. $\Gamma_{g,q}$ and $\gamma_{g,q}$ are, respectively, transverse and longitudinal relaxation rates in the gain and absorber media, and $\omega_{g,q}$ describe the shift of the central frequencies of the gain and absorption lines from the reference frequency. Here the index g (q) corresponds to the gain (absorber) medium. The main role of the linear filtering term $\gamma^{-1}dA\,(t)\,/(dt)$ is to regularise the system by converting delay algebraic-differential equations into DDEs. The parameters γ and ω_0 represent width and detuning of the central frequency of the linear filter. In order minimise the effect of the linear filter on the system's dynamics in numerical simulations we choose $\gamma\gg\Gamma_g$. Note that in the case of homogeneous broadening with $\omega_{g,q}=0$ equations (12)–(16) can be transformed into the standard DDE mode-locking model [24–26] by means of adiabatic elimination of polarisations $P_{g,q}$.

We further assume that the effect of inhomogeneous broadening on the dynamics of population difference is much weaker than its effect on the polarisation dynamics [7,10]. Then, implying that g_0 and q_0 are frequency independent, we assume $G(t)$ and $Q(t)$ to be frequency independent as well and apply the spectral method to obtain the following truncated system

$$\frac{dA}{dt}+(\gamma-i\omega_0)A=\sqrt{\kappa}\gamma\left[A\,(t-\tau)+P_{0q}+P_{0g}\right], \tag{17}$$

$$\frac{dP_{0q}}{dt}=(-\Gamma_q+i\omega_{0q})P_{0q}+i\sigma_qP_{1q} +\Gamma_q(e^{-Q/2}-1)A(t-\tau), \tag{18}$$

$$\frac{dP_{1q}}{dt}=-\left(\Gamma_q+\sqrt{2}p_{2q}\sigma_q+i\omega_{0q}\right)P_{1q}+i\sigma_qP_{0q}, \tag{19}$$

$$\frac{dP_{0g}}{dt}=(-\Gamma_g+i\omega_{0g})P_{0g}+i\sigma_gP_{1g} +\Gamma_g(e^{G/2}-1)\left[A(t-\tau)+P_{0q}\right], \tag{20}$$

$$\frac{dP_{1g}}{dt}=\left(-\Gamma_g-\sqrt{2}p_{2g}\sigma_g+i\omega_{0g}\right)P_{1g}+i\sigma_gP_{0g}. \tag{21}$$

$$\frac{dQ}{dt}=q_0-\gamma_qQ+s|A(t-\tau)+P_{0q}|^2 -s|A(t-\tau)|^2, \tag{22}$$

$$\frac{dG}{dt}=g_0-\gamma_gG-|A(t-\tau)+P_{0g}+P_{0q}|^2 +|A(t-\tau)+P_{0q}|^2, \tag{23}$$

where $P_{0,1}$ represent the zeroth- and first-order moments of polarisation, while all other moments satisfying

differential equations

$$\frac{dP_m}{dt} = (-\Gamma + i\omega_0)P_m + i\sigma(\sqrt{m}P_{m-1} + \sqrt{m+1}P_{m+1}), \tag{24}$$

are eliminated adiabatically. The coefficients p_2 in equations (19) and (21) can be approximated by setting $P_{M+1} = 0$ with M large enough. Then from equation (24) we get $P_M = ip_M P_{M-1}$ with $p_M = \sqrt{M}\sigma/(\Gamma - i\omega_0)$ and $P_m = ip_m P_{m-1}$ for all $2 < m < M-1$ with recursive relationship

$$p_m = \frac{\sqrt{m}\sigma}{\Gamma + i\omega_0 + \sqrt{m+1}\sigma p_{m+1}}.$$

Therefore, for $\omega_0 = 0$ we can see that $p_2 > 0$ and the main effect of the higher moments of polarisation is that they increase the relaxation rate of the first moment of polarisation for higher values of σ so that it becomes larger than relaxation rate of the zeroth-order moment of polarisation.

In the particular case when inhomogeneous broadening is present only in the gain medium we set $\sigma_q = 0$ in the absorber medium. Furthermore, in this case without the loss of generality we can assume that $\omega_{0q} = 0$. Then eliminating adiabatically the variable P_{0q} from equation (18) we obtain the relations $P_{0q} = (e^{-Q(t)/2} - 1)A(t-\tau)$ and $P_{1q} = 0$, which lead to the following equations for the complex field envelope A, saturable gain G, and saturable loss Q:

$$\gamma^{-1}\frac{dA}{dt} + A = \sqrt{\kappa}\left[e^{-Q/2}A(t-\tau) + P_{0g}\right], \tag{25}$$

$$\frac{dG}{dt} = g_0 - \gamma_g G - \left(|e^{-Q/2}A(t-\tau) + P_{0g}|^2 - e^{-Q}|A(t-\tau)|^2\right), \tag{26}$$

$$\frac{dQ}{dt} = q_0 - \gamma_q Q - s\left(1 - e^{-Q}\right)|A(t-\tau)|^2. \tag{27}$$

Combining these three equations with equations (20) and (21) evaluated at $\omega_{0g} = 0$ we get DDE model of a laser with inhomogeneously broadened gain line and adiabatically eliminated polarisation in the absorbing medium. The lasing threshold in this laser can be expressed as

$$\sqrt{\kappa}\exp\left(\frac{g_0}{2\gamma_g} - \frac{q_0}{2\gamma_q}\right) = 1 + \frac{\sigma_g^2}{\tilde{\Gamma}^2}\left[1 - \sqrt{\kappa}\exp\left(-\frac{q_0}{2\gamma_q}\right)\right] \geq 1,$$

where $\tilde{\Gamma}^2 = \Gamma_g[\Gamma_g + \sigma_g p_{2g}]$, i.e. inhomogeneous broadening in the gain medium leads to an increase of the lasing threshold.

Similarly to equations (25)–(27) the equations governing the time evolution of the complex field envelope A and saturable gain G can be derived for the case when inhomogeneous broadening is present in the absorber medium only. Setting $\sigma_g = \omega_{0g} = \omega_{0q} = 0$, $P_{1g} = 0$, and eliminating adiabatically the variable P_{0g} we get $P_{0g} = \left(e^{G/2} - 1\right)[A(t-\tau) + P_{0q}]$ and

$$\gamma^{-1}\frac{dA}{dt} + A = \sqrt{\kappa}\left[e^{G/2}A(t-\tau) + P_{0q}\right], \tag{28}$$

$$\frac{dG}{dt} = g_0 - \gamma_g G - \left(e^G - 1\right)|A(t-\tau) + P_{0q}|^2. \tag{29}$$

Combining these two equations with equations (18), (19) and (22) evaluated at $\omega_{0q} = 0$ to these two equations we get the DDE model of a laser with inhomogeneously broadened absorber and homogeneously broadened gain lines. We note that in this model the spectral filtering is attributed to the linear filtering section instead of the gain section. Therefore, in contrast to the model (12)–(16), where γ is introduced for regularisation purposes, now spectral filter is affecting the pulse width. In this situation we employ a commonly adopted procedure by choosing γ equal to Γ_g used in equations (12)–(16), and by replacing a nonlinear filter with a linear filter [24–26,29–31]. The lasing threshold of the central mode in this case can be expressed as

$$\sqrt{\kappa}\exp\left(\frac{g_0}{2\gamma_g} - \frac{q_0}{2\gamma_q}\right) = \frac{1 + \sigma_q^2/\tilde{\Gamma}^2}{1 + \sigma_q^2 e^{q_0/(2\gamma_q)}/\tilde{\Gamma}^2} \leq 1,$$

where $\tilde{\Gamma}^2 = \Gamma_q[\Gamma_q + \sigma_q p_{2q}]$, i.e. inhomogeneous broadening in the absorber medium leads to a decrease of the linear threshold of the central mode located in the middle of the spectral profile of the absorption line.

4 Numerical results

4.1 TWE model

We solve equations (8)–(10) for the two-section laser with a gain and an absorber section using the discretisation scheme similar to the one reported in [29,30], which is outlined in Appendix B. Since the number of moments reaches up to $M = 200$, we use parallelisation techniques to speed up our simulations.

In numerical simulations the parameter values of equations (8)–(10) were similar to those used earlier for modelling of monolithic semiconductor lasers with homogeneously broadened gain and absorption lines [29,30]. In particular, the reflectivities of the laser facets were assumed to be equal, $\kappa_1 = \kappa_2 = 0.3$. Furthermore, for simplicity we assume that $\omega_{g0} = \omega_{q0} = 0$ and that all the linear losses take place on the laser facets, i.e., $\beta_{g,q} = 0$. The remaining parameters of the gain (absorber) sections are: normalised pump rate $n_0 = 10\,\mathrm{ns}^{-1}$ (linear absorption rate $n_0 = 0.16\,\mathrm{ps}^{-1}$), longitudinal relaxation time $\gamma_N^{-1} = 1\,\mathrm{ns}$ ($\gamma_N^{-1} = 10\,\mathrm{ps}$), transverse relaxation time $\Gamma^{-1} = 250\,\mathrm{fs}$ ($\Gamma^{-1} = 250\,\mathrm{fs}$), and normalised saturation parameter $s = 1$ ($s = 5$). The length of the gain and absorber sections normalised to the group velocity of light in this sections are 10 ps and 2.5 ps, respectively.

A typical bifurcation tree obtained by plotting local maxima of the laser intensity time trace calculated for

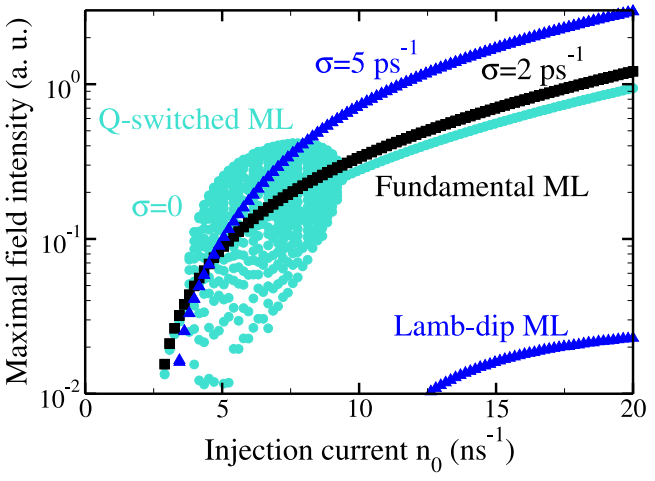

Fig. 1. Bifurcation tree obtained by numerical integration of equations (8)–(10). Local maxima of the field intensity are plotted for different values of the pump parameter n_0 in the gain medium. Cyan circles correspond to $\sigma = 0$, black rectangles – to $\sigma = 2\,\mathrm{ps}^{-1}$, and blue triangles – to $\sigma = 5\,\mathrm{ps}^{-1}$ in a laser with inhomogeneously broadened gain and absorber lines. Blue triangles in the lower right corner of the figure indicate the peak power of the satellite pulse that appears at the trailing edge of the main pulse. Other parameter values are given in the beginning of Section 4.1.

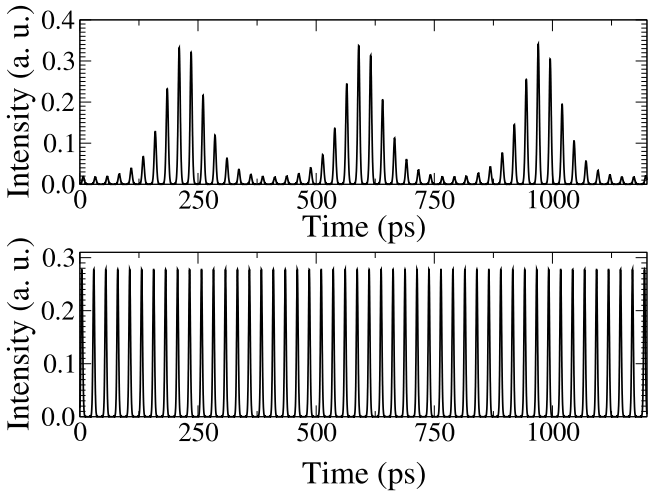

Fig. 2. Right: time traces of Q-switched regime (top) and fundamental mode-locking regime (bottom) calculated for $\sigma = 0$. Other parameter values are as in Figure 1.

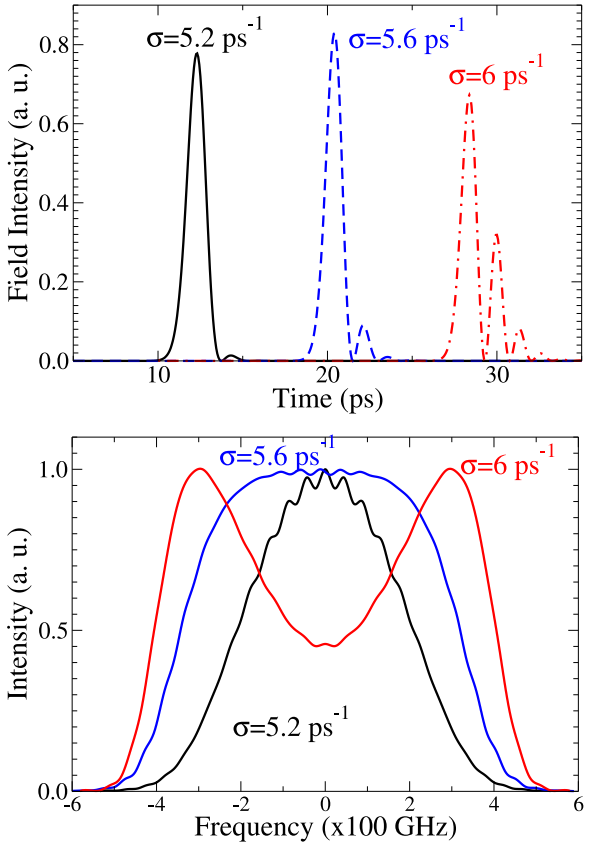

Fig. 3. Pulses (top) and optical spectra (bottom) in a laser with inhomogeneously broadened gain and absorber lines having equal linewidth $\sigma = 5.2\,\mathrm{ps}^{-1}$, $\sigma = 5.6\,\mathrm{ps}^{-1}$, and $\sigma = 6\,\mathrm{ps}^{-1}$. Optical spectrum of the pulse is obtained using the discrete Fourier transform of a single period of the periodic ML solution. Here, the pump parameter in the gain medium is $n_0 = 10\,\mathrm{ns}^{-1}$, and other parameters are as in Figure 1.

increasing values of the pump parameter n_0 in the gain medium in a laser with homogeneously broadened gain and absorber lines, $\sigma_g = \sigma_q = 0$, is shown by cyan circles in Figure 1. It can be seen that soon after the lasing threshold a regime with periodic laser intensity undergoes an instability leading to a Q-switched mode-locking regime corresponding to a cloud of points in Figure 1. Quasiperiodic intensity time trace of the latter regime is shown in the top panel of Figure 2. At even larger pumps a fundamental mode-locking regime illustrated in the bottom panel of Figure 2 becomes stable. Black rectangles (blue triangles) in Figure 1 are obtained by increasing the pump parameter n_0 at fixed and equal inhomogeneous broadening linewidths, $\sigma_g = \sigma_q = \sigma$, in the gain and absorber media, $\sigma = 2\,\mathrm{ps}^{-1}$ ($\sigma = 5\ \mathrm{ps}^{-1}$). It can be seen that the lasing threshold remains almost independent of σ, however, the Q-switching instability is gone for $\sigma \geq 2\,\mathrm{ps}^{-1}$. Therefore, we conclude that inhomogeneous broadening can lead to a suppression of this instability, which is in agreement with the experimental data on quantum-dot mode-locked lasers [33] and with the general considerations of reference [15].

For sufficiently large σ in the gain and absorber media small satellite pulses can appear at the trailing edge of the main mode-locked pulse. This can be seen in the top panel of Figure 3 illustrating fundamental mode-locking regimes with one, two and three additional satellite pulses. The corresponding spectra shown in Figure 3 (bottom) become wider with the increase of σ and eventually a Lamb dip [34], similar to that reported earlier in actively mode-locked quantum-dot lasers [15], is formed in the middle of the pulse spectrum. Further increase of the inhomogeneous linewidth leads to a separation of the spectral comb into two symmetric combs with positive and negative central frequencies and subsequent degradation

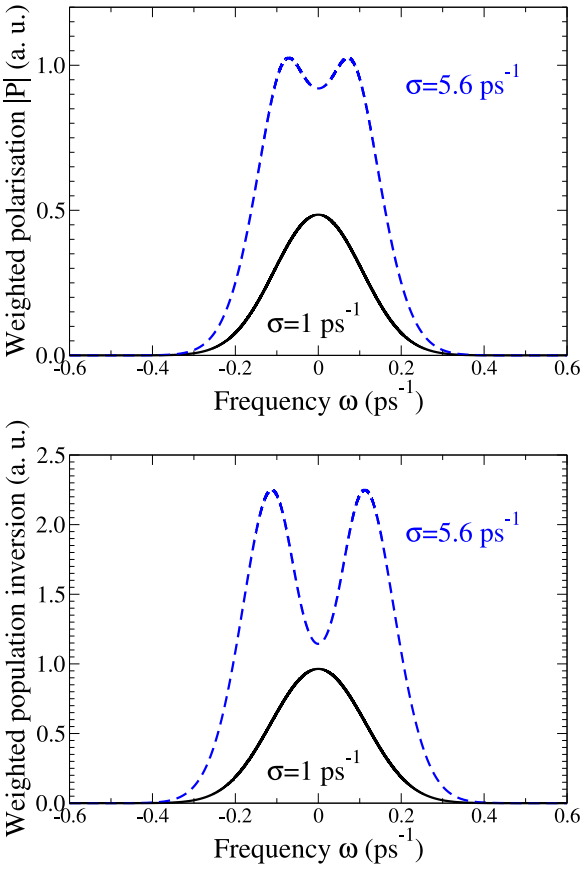

Fig. 4. Reconstructed polarisation (top) and population difference (bottom) functions $|P^+(\omega, t_{\rm pulse}, L)\phi_0(\omega)|$, $N(\omega, t_{\rm pulse}, L)\phi_0(\omega)$ at the end of the absorber section ($z = L$, output edge) at the moment of maximal pulse intensity $t = t_{\rm pulse}$, where P, N approximate solutions of (1)–(3), and ϕ_0 is defined by (5), in a laser with inhomogeneously broadened gain and absorber lines having equal linewidth $\sigma = 1\,{\rm ps}^{-1}$ and $\sigma = 5.6\,{\rm ps}^{-1}$. Other parameters are as in Figure 3.

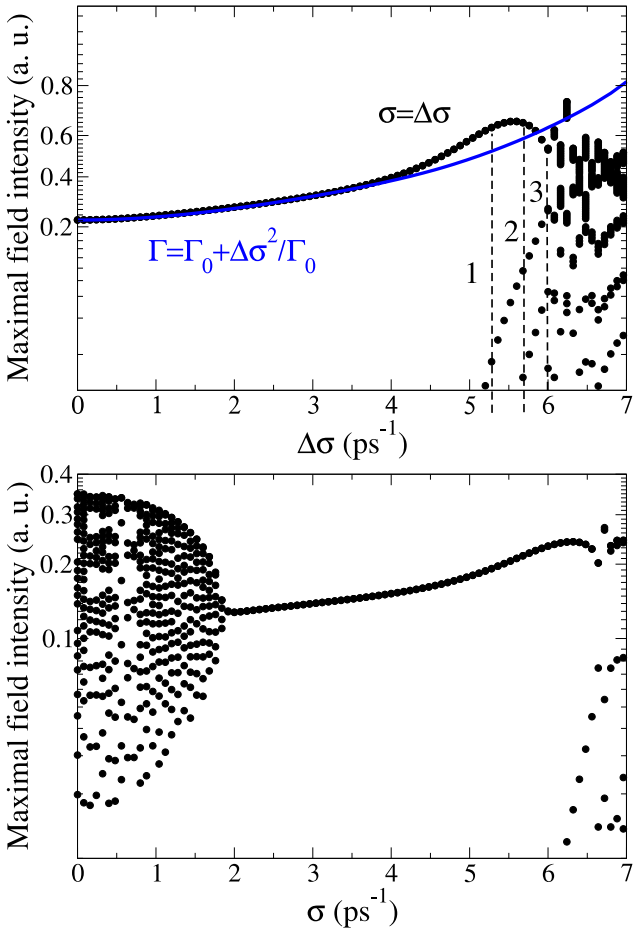

Fig. 5. Bifurcation diagrams similar to that shown in Figure 1, obtained by increasing the parameter σ in both media. Top: black dots show local maxima of the field intensity calculated by changing σ with fixed normalised pump rate $n_0 = 10\,{\rm ns}^{-1}$. Blue line represents intensity maxima of fundamental mode-locking solutions calculated by changing $\Gamma_g = \Gamma_q$ in a laser with homogeneously broadened gain and absorption lines. Dashed lines denote values of σ where new satellite pulses appear. Bottom: Same as black dots in the upper panel, but for $n_0 = 6\,{\rm ns}^{-1}$. Other parameters are as in Figure 1.

of mode-locking via an instability which is referred here as the "Lamb dip instability". Figure 4 demonstrates the polarisation P^+ and population difference N weighed by the exponential function ϕ_0 as the function of frequency ω. One can see that for sufficiently large inhomogeneous broadening width σ spectral holes appear in these profiles. Comparing this figure with Figure 3 (bottom) we can observe that for increasing σ the spectral hole in the profile of $P^+\phi_0$ and $N\phi_0$ precedes the formation of the Lamb dip in the pulse spectral profile.

Evolution of fundamental mode-locked regime with the increase of the inhomogeneous broadening widths σ in the gain and absorber media is illustrated by the top panel of Figure 5. Black circles in this figure indicate local maxima of the field intensity calculated for different values of σ with fixed normalised pump parameter $n_0 = 10\,{\rm ns}^{-1}$. It can be seen that the peak power of the mode-locked pulse increases with σ within the interval $\sigma \in [0, 5]\,{\rm ps}^{-1}$, while for $\sigma > 5\,{\rm ps}^{-1}$ additional satellite pulses shown in Figure 3 (top) appear on the trailing edge of the pulse. Blue line in Figure 5 (top) indicates the linear increase of the pulse intensity with the homogeneous broadening width Γ in the absence of inhomogeneous broadening, $\sigma = 0$. It follows from (11) that when $\sigma = \Delta\sigma$ is sufficiently small, the effect of inhomogeneous broadening is analogous to the increase of the homogeneous broadening width from Γ_0 to $\Gamma = \Gamma_0 + \Delta\sigma^2/\Gamma_0$. On the other hand, for larger $\Delta\sigma$ the pulse width continues to decrease for increasing homogeneous broadening, while mode-locked regime eventually looses stability for increasing inhomogeneous broadening. Bottom panel of Figure 5 presents a similar bifurcation diagram calculated for smaller value of the pump parameter, $n_0 = 6\ {\rm ns}^{-1}$ corresponding to a stable Q-switched mode-locking regime in the absence of inhomogeneous broadening. It can be seen that increasing the inhomogeneous broadening width in the gain medium up to $\sigma \approx 2\ {\rm ps}^{-1}$ leads to a suppression of Q-switching instability and a transition to a stable fundamental mode-locking regime. The latter regime remains stable for $2 \le \sigma < 6\ {\rm ps}^{-1}$.

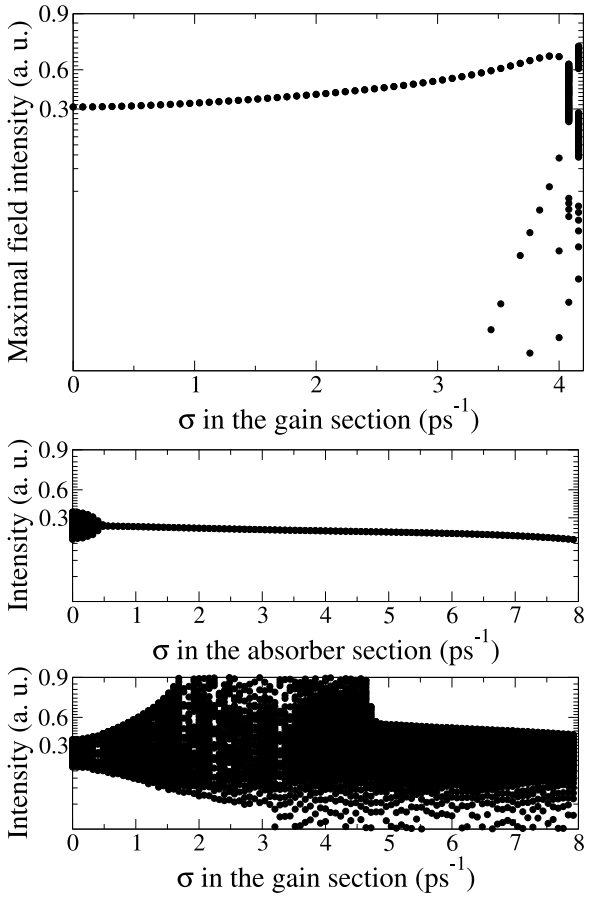

Fig. 6. Bifurcation diagrams obtained numerically by changing the parameter σ in the gain (top, bottom)/absorber (center) medium in a laser with homogeneously broadened absorption (top, bottom)/gain (center) line. Normalized pump rates are $n_0 = 20\,\mathrm{ns}^{-1}$ (top) and $n_0 = 9\,\mathrm{ns}^{-1}$ (center, bottom). Other parameters are as in Figure 1. In the bottom panels the Intensity labels denote for brevity maximal field intensity as in the top panel.

It follows from the top panel of Figure 6 that the Lamb-dip instability appears due to the inhomogeneous broadening of the gain line, while the suppression of Q-switching is due to inhomogeneous broadening of the absorber line, see central panel of Figure 6. The absence of instability for high values of the parameter σ in the absorber medium (see central panel of Fig. 6) suggests that the inhomogeneous broadening in the absorber medium does not participate in the development of Lamb-dip instability. On the other hand, the diagram shown in bottom panel of Figure 6 indicates that inhomogeneous broadening of the gain medium does not suppress the Q-switching instability of mode-locked regime, but on the contrary enhances this instability.

In order to study the effect of the inhomogeneous broadening in the gain and absorber media on the characteristics of mode-locked pulses we plot in Figure 7 the dependence of their full-width at half-maxima, spectral width, energy, and the time-bandwidth product as functions of the inhomogeneous broadening width σ. It can be seen from this figure that the pulse width decreases and the spectral width increases with increasing σ. This is in agreement with intuitive expectations as well as with the theoretical results obtained for actively mode-locked quantum-dot lasers [15]. The time-bandwidth product remains almost constant for $\sigma < 5\,\mathrm{ps}^{-1}$, and increases drastically together with the spectral width for higher σ. The pulse energy decreases monotonically with increasing σ.

Finally, one can notice from Figure 1 that an increase of inhomogeneous broadening linewidth σ can lead to a slight increase of the lasing threshold. Figure 8 (top) shows a more dramatic increase of the lasing threshold obtained for faster gain relaxation rate $\gamma_N = 125\,\mathrm{ps}^{-1}$. Furthermore, a comparison of Figure 8 (bottom) and Figure 1 shows that for the faster gain relaxation rate $\gamma_N = 125\,\mathrm{ps}^{-1}$ the Lamb-dip instability of mode-locking regime appears at higher values of σ then for slower relaxation rate $\gamma_N = 10\,\mathrm{ps}^{-1}$.

4.2 DDE model

First, we simulate the DDE model (12)–(16) of a laser with inhomogeneously broadened gain and absorption lines with the parameter values close to those of the TWE model: $\tau = 25$ ps, $\kappa = 0.3$, $\Gamma_g^{-1} = \Gamma_q^{-1} = 250$ fs, $\gamma_g^{-1} = 1$ ns, $\gamma_q^{-1} = 5$ ps, $\gamma^{-1} = 25$ fs, $s = 10$, $g_0 = 6\,\mathrm{ns}^{-1}$, and $q_0 = 0.1\,\mathrm{ps}^{-1}$. The dependence of the pulse peak intensity on the inhomogeneous broadening width $\sigma_g = \sigma_q \equiv \sigma$ obtained with the help of the DDE-BIFTOOL software package [35] is presented in the top panel of Figure 9. It can be seen that the bifurcation diagram in this figure is similar to that obtained by numerical simulation of the TWE model, see Figure 5 (bottom).

In order to perform numerical analysis of the Lamb-dip instability we simulate the DDE model with inhomogeneously broadened gain line and adiabatically eliminated polarisation in the absorber medium, equations (25)–(27), (20), and (21). We increase carrier relaxation rate up to $\gamma_g^{-1} = 500$ ps and, using the DDE-BIFTOOL software package, perform a continuation of the mode-locked solution along the parameter σ_g, see Figure 9 (bottom). The presence of additional lines in the bottom right corner of the figure indicates that similarly to the results of numerical simulation with the TWE model shown in the bottom panel of Figure 5 the increase of σ_g leads to formation of small satellite pulses behind the main mode-locked pulse. The branch of mode-locked solutions in Figure 5 (bottom) ends up at a saddle-node (fold) bifurcation point, where the negative real eigenvalue with smallest absolute value becomes zero.

Top panel of Figure 10 presents a branch of mode-locking solutions of the DDE model (28), (29), (18), (19), and (22) with homogeneously broadened absorber line and adiabatically eliminated polarisation in the gain medium. As we previously noted the spectral filtering in this model is performed by a linear filter with the bandwidth $\gamma^{-1} = 250$ ns. The part of this branch between bifurcation points A and B shown by dotted line is unstable with respect to Q-switching instability. In the bottom panel of Figure 10

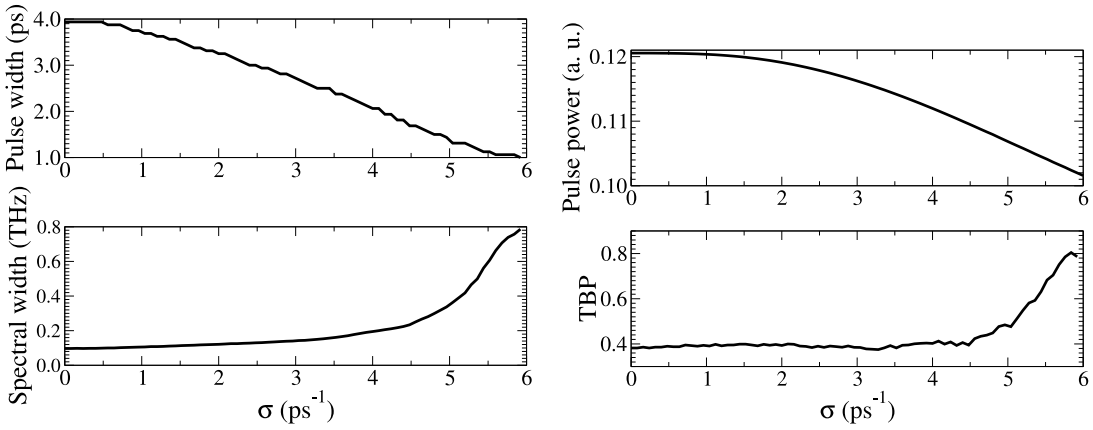

Fig. 7. Left: full-width at half-maximum of the mode-locked pulses (top) and their spectral width (bottom) as functions of equal inhomogeneous broadening widths σ in the gain and absorber media. $n_0 = 10\,\mathrm{ns}^{-1}$ in the gain medium. Other parameters are as in Figure 1. Right: pulse energy (top) and time-bandwidth product versus inhomogeneous broadening linewidth in the gain medium. $n_0 = 10\,\mathrm{ns}^{-1}$ in the gain medium. Other parameters are as in Figure 1.

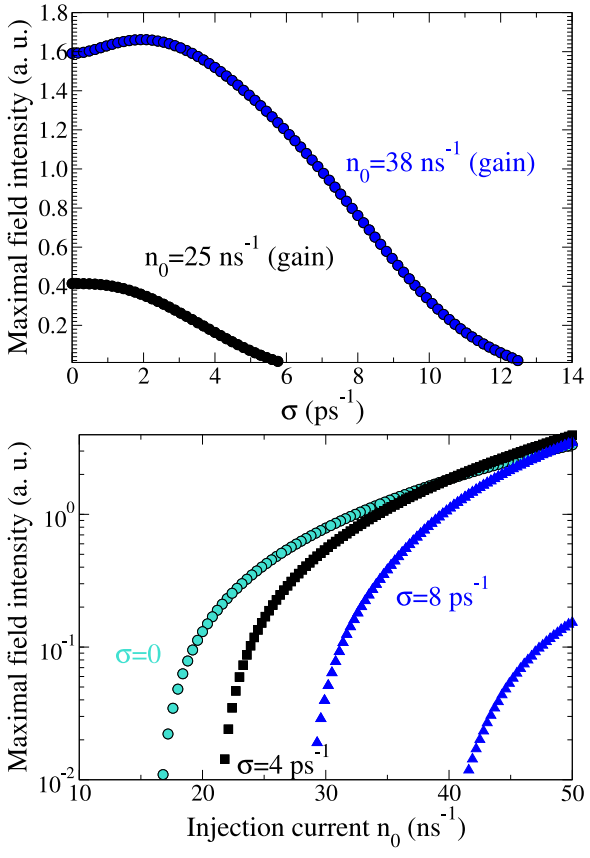

Fig. 8. Top: bifurcation diagram obtained numerically by changing the parameter σ in gain and absorber media for pump rates $n_0 = 25\,\mathrm{ns}^{-1}$ and 38 ns^{-1} in the gain medium. Bottom: bifurcation diagram obtained numerically by changing the parameter n_0 in the gain medium for $\sigma = 0$ (circles), $\sigma = 4\,\mathrm{ps}^{-1}$ (rectangles), and $\sigma = 8\,\mathrm{ps}^{-1}$ (triangles) in both media, $\gamma_N = 125\,\mathrm{ps}^{-1}$ in the gain medium, $n_0 = -320\,\mathrm{ns}^{-1}$ in the absorber medium. Other parameters are as in Figure 1.

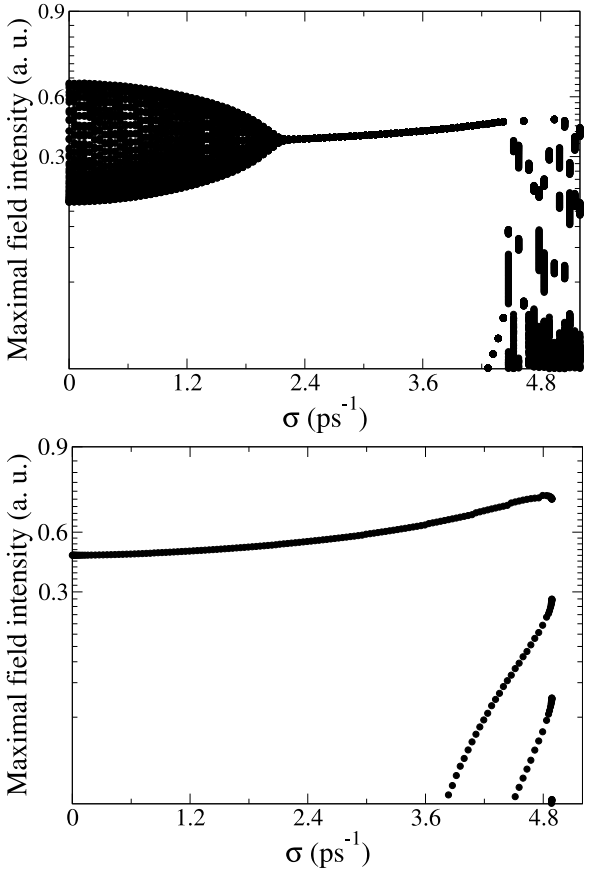

Fig. 9. Top: bifurcation diagram obtained numerically by changing the parameter $\sigma_g = \sigma_q = \sigma$ in both laser media using the DDE model (12)–(16). Bottom: bifurcation diagram obtained with the help of DDE-BIFTOOL by changing the parameter $\sigma_g = \sigma$ in the DDE model (25)–(27), (20), and (21). Here, the unsaturated gain parameter is $g_0 = 6\,\mathrm{ns}^{-1}$, and other parameters can be found in the beginning of Section 4.2.

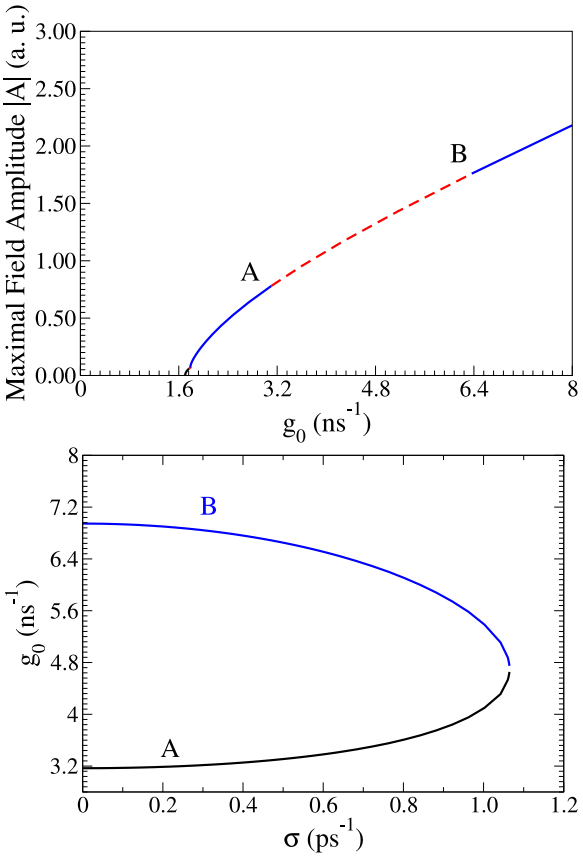

Fig. 10. Top: bifurcation diagram obtained using the DDE-BIFTOOL by continuing the branch of the mode-locking regime along the parameter g_0 of the DDE model (28), (29), (18), (19), and (22) with $\sigma_q = 0$. Solid lines indicate stable solutions, while dashed line indicates unstable ones. $\gamma^{-1} = 250$ ns. Bottom: two-parameter bifurcation diagram obtained using the DDE-BIFTOOL by following the Q-switching instability bifurcation points A and B along the parameter $\sigma_q = \sigma$ of the DDE model (28), (29), (18), (19), and (22). Other parameter are as in Figure 9.

the critical values of the pump parameter g_0 corresponding to the Q-switching instability bifurcation points are shown as functions of the inhomogeneous broadening width $\sigma_q = \sigma$ of the absorption line. It can be seen that with increasing σ the two bifurcation points collide and disappear, and the mode-locking solution branch becomes stable within the whole range of pump parameters shown in Figure 10 (top).

Finally, we note that although the approximation of slow evolution of the population differences underlying the DDE model (12)–(16) is based on qualitative considerations, our numerical simulations indicate that the results obtained using the DDE model are in good qualitative agreement with those of the TWE model. This could be understood by taking into account the fact that the characteristic times of the population differences evolution, $1/\gamma_{g,q}$, are usually much larger than those of the field envelope, $1/\gamma$, and polarisations, $1/\Gamma_{g,q}$. In particular, the carrier dynamics during the fast stage of passive mode-locking [26] is still much slower than the polarisation dynamics and has weak effect on the evolution of polarisation.

5 Conclusion

We have studied numerically two-level TWE model of a passively mode-locked laser with inhomogeneousy broadened gain and absorption lines. We have proposed an efficient spectral method for numerical integration of this model, and implemented this method using parallel computation techniques. We have studied the effect of the inhomogeneous broadening on the characteristics of the fundamental mode-locking regime. It follows from our analysis that, alongside with the carrier dynamics processes in the gain medium, see e.g. [30,33,36], inhomogeneous broadening may lead to a suppression of Q-switching instability in mode-locked quantum-dot lasers. This is in agreement with qualitative considerations, which suggest the enhancement of the gain saturation and suppression of Q-switching due to inhomogeneous broadening [37]. We have shown that equal inhomogeneous broadening widths in both laser media can lead to the increase of the lasing threshold, pulse intensity and spectral width, and to the decrease of the pulse width and the pulse power. Moreover, small inhomogeneous broadening has the effect on pulse characteristics similar to that of homogeneous broadening, whereas large inhomogeneous broadening in the absorber (gain) medium leads to a suppression of Q-switching instability (the formation of the Lamb dip in the spectral profile of the pulse and the degradation) of the mode-locking regime. We have demonstrated that the increase of the longitudinal relaxation rate in the gain medium leads to stabilisation of the fundamental mode-locking regime for strong inhomogeneous broadening and to further increase of the lasing threshold.

We have derived a simplified DDE model of an inhomogeneously broadened laser which demonstrates dynamical behaviour qualitatively similar to that of the TWE model. Using the DDE model we have shown that the degradation of mode-locked regime at sufficiently large values of the inhomogeneous broadening linewidth in the gain medium takes place after a fold bifurcation where the stable branch of fundamental mode-locked solutions disappears. Finally, we have demonstrated that with the increase of inhomogeneous broadening linewidth in the absorber medium two bifurcation points responsible for the appearance to the Q-switching instability of mode-locked regime collide and disappear, leading to elimination of this instability by inhomogeneous broadening.

The authors acknowledge the support of SFB 787 of the DFG, project B5. A.G.V. acknowledges the support by Grant No. 14-41-00044 of the Russian Science Foundation.

Author contribution statement

A.G.V. proposed and directed the study. A.G.V. and A.P. contributed equally to the formulation of the TWE model,

derivation of the DDE model, analysis of the models and interpretation of the results, and to the preparation of the manuscript. A.P. proposed and applied the Galerkin method using the basis of Hermite functions for the TWE model, developed discretisation and parallelisation schemes, performed all numerical simulations, and prepared all the Figures.

Appendix A: Derivation of the DDE model

To derive a DDE model of a ring passively mode-locked laser taking into account medium polarisation dynamics we use the approach similar to that proposed in [24–26]. We start with the unidirectional travelling wave equations describing the space-time evolution of the complex electrical field envelope E, complex two-level polarisation P, and real population difference N in the gain and absorber media written out in co-moving coordinate frame $z + t \to z$, $t \to t$:

$$\begin{aligned}
&\frac{\partial E}{\partial z} = P,\\
&\frac{\partial P}{\partial t} = (-\Gamma + i\omega)P + \frac{\Gamma}{2}EN,\\
&\frac{\partial N}{\partial t} = n_0 - \gamma_N n - s(EP^* + PE^*) = n_0 - \gamma_N n - s\frac{\partial |E|^2}{\partial z},
\end{aligned}$$

where the equation for the electric field envelope E can we rewritten in the form:

$$\frac{\partial^2 E}{\partial t \partial z} + (\Gamma - i\omega)\frac{\partial E}{\partial z} = \frac{\Gamma}{2}EN. \tag{A.1}$$

Assuming that the time evolution of the population difference N is much slower than that of the field envelope E we apply Fourier-transform to (A.1) considering $N(t, z)$ to be independent of time t. Then we obtain

$$2\pi i\xi\frac{d\tilde{E}}{dz} + (\Gamma - i\omega)\frac{d\tilde{E}}{dz} = \frac{\Gamma}{2}\tilde{E}N. \tag{A.2}$$

Integrating (A.2) along longitudinal coordinate z from the point z_1 at the beginning of the gain/absorber medium to the point z_2 at the end of the the medium we get

$$\begin{aligned}
\tilde{E}(\xi, z_2) &= \exp\left[\frac{\Gamma G}{2(\Gamma - i\omega + 2\pi i\xi)}\right]\tilde{E}(\xi, z_1)\\
&= \sum_{k=0}^{\infty}\frac{1}{k!}\left[\frac{\Gamma G}{2(\Gamma - i\omega + 2\pi i\xi)}\right]^k \tilde{E}(\xi, z_1),
\end{aligned} \tag{A.3}$$

where $G = \int_{z_1}^{z_2} N dz$. Therefore, by making the inverse Fourier transform of (A.3) we obtain

$$\begin{aligned}
E(t, z_2) &= E(t, z_1) + \frac{\Gamma G(t)}{2}\\
&\times \int_{-\infty}^{t} E(s, z_1)e^{(\Gamma - i\omega)(s-t)}\frac{I_1\left[\sqrt{(t-s)G(t)\frac{2\Gamma}{\Gamma - i\omega}}\right]}{\sqrt{(t-s)G(t)\frac{\Gamma}{2(\Gamma - i\omega)}}}ds,
\end{aligned} \tag{A.4}$$

where I_1 is the first order Bessel function.

Finally, assuming that the time evolution of $G(t)$ is slow we eliminate distributed delay we rewrite equation (A.4) as the following chain of equations

$$\begin{aligned}
&E(t, z_2) = E(t, z_1) + P_1(t),\\
&\frac{dP_1(t)}{dt} = (-\Gamma + i\omega)P_1(t) + \frac{\Gamma G(t)}{2}(E(t, z_1) + P_2(t)),\\
&\frac{dP_2(t)}{dt} = (-\Gamma + i\omega)P_2(t) + \frac{\Gamma G(t)}{2 \times 2}(E(t, z_1) + P_3(t)),\\
&\frac{dP_3(t)}{dt} = (-\Gamma + i\omega)P_3(t) + \frac{\Gamma G(t)}{3 \times 2}(E(t, z_1) + P_4(t)),\\
&\qquad\qquad \cdots\\
&\frac{dP_k(t)}{dt} = (-\Gamma + i\omega)P_k(t) + \frac{\Gamma G(t)}{2k}(E(t, z_1) + P_{k+1}(t)),\\
&\qquad\qquad \cdots
\end{aligned}$$

where P_m are auxiliary variables describing the polarisation at the point z_2. Assuming $G(t)/2 \ll 1$, we can truncate the system at any $k \geq 1$. For higher $G(t) \sim 1$ we improve the approximation by keeping a single polarisation equation for P_1 with all other auxiliary variables P_m $(m > 1)$ eliminated adiabatically:

$$\frac{dP_1(t)}{dt} = (-\Gamma + i\omega)P_1(t) + \Gamma(e^{G(t)/2} - 1)E(t, z_1).$$

This equation is responsible for nonlinear spectral filtering approximating the effect of two-level polarisation on the laser dynamics at small $G(t)$.

Using the above approximation, we write the following equation for the time evolution of the complex electric field envelope in a two-section passively mode-locked laser

$$\frac{dA}{dt} + (\gamma - i\omega_0)A = \sqrt{\kappa}\gamma\left[A(t - \tau) + P_q(t) + P_g(t)\right], \tag{A.5}$$

where $P_g(t)$ and $P_q(t)$ describe the polarisation of the gain and absorber medium, respectively. Equation (A.5) together with equations (13)–(16) gives us a DDE model for a homogeneously broadened mode-locked laser. By setting $\omega_{0g} = \omega_{0q} = 0$ and performing adiabatic elimination of the variables P_g and P_q we obtain from this model the standard DDE mode-locking model of references [24–26].

Appendix B: Numerical solution of the TWE

For spatial discretisation of the TWE we use the method developed for homogeneously broadened passively

$$\frac{\partial p^{\pm}_{m,k}}{\partial t}(t) \approx (-\Gamma + i\omega_0)p^{\pm}_{m,k} + i\sigma_D(\sqrt{m}p^{\pm}_{m-1,k} + \sqrt{m+1}p^{\pm}_{m+1,k}) + \Gamma G_{m,k}(t)\frac{E^{\pm}(t,z_k)(1+e^{-\frac{\beta\Delta z}{2}}) + (1-\frac{\beta\Delta z}{4})p^{\pm}_{0,k}(t)}{2} \tag{B.3}$$

$$\frac{\partial G_{m,k}}{\partial t} \approx g_m - \gamma_N G_{m,k} - \frac{s}{2}\mathrm{Re}\big((p^{-*}_{m,k}E^{-}(t,z_{k+1}) + p^{+*}_{m,k}E^{+}(t,z_k))(1+e^{-\frac{\beta\Delta z}{2}}) + \left(1-\frac{\beta\Delta z}{4}\right)(p^{-*}_{m,k}p^{-}_{0,k} + p^{+*}_{m,k}p^{+}_{0,k})\big) \tag{B.4}$$

mode-locked multisection semiconductor laser [29,30]. We divide the laser into K segments of size $\Delta z = l/K$, and integrate equation (8) along the characteristics to obtain the following second-order accurate approximation at the end-points of the segments

$$E^{+}(t+\Delta z, z_{k+1}) = E^{+}(t,z_k)e^{-\frac{\beta\Delta z}{2}} + \left(1-\frac{\beta\Delta z}{4}\right)p^{+}_{0,k}(t) + O(\Delta z^3), \tag{B.1}$$

$$E^{-}(t+\Delta z, z_k) = E^{-}(t,z_{k+1})e^{-\frac{\beta\Delta z}{2}} + \left(1-\frac{\beta\Delta z}{4}\right)p^{-}_{0,k}(t) + O(\Delta z^3). \tag{B.2}$$

After that we denote

$$p^{\pm}_{m,k} = \int_{z_k}^{z_{k+1}} P^{\pm}_m\left(t-\frac{\Delta z}{2}, z\right)dz,$$

$$G_{m,k} = \int_{z_k}^{z_{k+1}} N_m\left(t-\frac{\Delta z}{2}, z\right)dz,$$

and integrate equations (10), (9) for $P^{\pm}_m(t-\Delta z/2, z), N^{\pm}_m(t-\Delta z/2, z)$ over $z \in [z_k, z_{k+1}]$, approximating the integrals of multiplications using trapezoid method, hence obtaining second-order approximations

See equations (B.3) *and* (B.4) *above.*

For discretisation of $p^{\pm}_{m,k}$ in time we use the Crank-Nicolson method with time step $\Delta t = \Delta z$. We consider equations for $p^{\pm}_{m,k}$, approximate $G_{m,k}(t_{n+1})$ using explicit method [32], and for each n, k, m we obtain the following system of linear algebraic equations (SLAE) with quasi-tridiagonal matrix

$$A^{\pm}_{m,k,n}p^{\pm}_{m-1,k,n+1} + B^{\pm}_{m,k,n}p^{\pm}_{m,k,n+1} + C^{\pm}_{m,k,n}p^{\pm}_{m+1,k,n+1} + D^{\pm}_{m,k,n}p^{\pm}_{0,k,n+1} = F^{\pm}_{m,k,n}.$$

We look for the solution of the equations for $m = 1, \ldots, M$ in the form $p^{\pm}_{m,k,n+1} = X_{m,k,n} - Y_{m,k,n}p^{\pm}_{0,k,n+1}$ using a modified algorithm of solution of SLAE with tridiagonal matrices. Then we solve two equations for $p^{\pm}_{0,k,n+1}$, $p^{\pm}_{1,k,n+1}$, propagate values of $p^{\pm}_{m,k,n+1}$ for $m > 1$, and use Crank-Nicolson method to find $G_{m,k}(t_{n+1})$.[1] Since the complexity of the algorithm of solution of SLAE with tridiagonal matrix is $O(M)$, the total complexity of the numerical algorithm is $O(MK^2T/l)$, where T is the total time of simulation. We note that the numerical scheme (B.1)–(B.4) is a second-order semi-implicit scheme suitable for stiff problems such as simulation of mode-locked lasers [29,32], and its algorithmic complexity remains linear in the number of moments M, while direct discretisation of the integral over polarisations (1) results in the full matrix in the equations (B.3)–(B.4), and inefficiency of the proposed scheme. Our aim was to develop a robust algorithm for our study, which is numerically stable over a wide realistic parameter range and for sufficiently large time steps $\Delta t = \Delta z$. Hence we did not investigate alternative approaches such as explicit approximation of polarisation terms in (B.3)–(B.4) that come from the direct discretisation of the integral in (1). Nevertheless, we assume that polarisations relax much faster than the populations differences, which leads to stiffness in the equations and numerical instability of explicit schemes.

We parallelise the numerical scheme (B.1)–(B.4) by considering each small section of a laser $[z_k, z_{k+1}]$ at the moment of time t_n as a cell that communicates with the other cells during the calculations. We place the neighbouring cells in a group and assign each group to a computing node, which can be another thread or an MPI process. We demonstrate the scheme of the calculation of the variables at each moment of time t_{n+1} for the case of two computing nodes on Figure B.1 (number of nodes $N_C = 2$). We can see that each cell k is connected to the two neighbouring cells in the variables $E^{\pm}_{k\pm1,n+1}$, which are obtained using simple rules (B.1)–(B.2) from the values of the variables $E^{\pm}_{k,n}, p^{\pm}_{0,k,n}$ at the moment of time t_n. Hence only one value should be sent to each neighbouring computing node from the current node at each time step, which is accomplished by sending the corresponding value of $E^{\pm}_{k,n+1}$ through a "ghost" cell, which, for example, can be responsible for sending and receiving MPI messages.

[1] We have found that such approach to $G_{m,k}(t_{n+1})$ is numerically stable for the parameters we used. In other situations it can be further improved by predictor-corrector steps, or made fully implicit by applying Crank-Nicolson method to $G_{m,k}(t_{n+1})$ instead of explicit approximation on the first step. The resulting equations are nonlinear and the matrix for the Newton iterations is block tridiagonal with the block size 4.

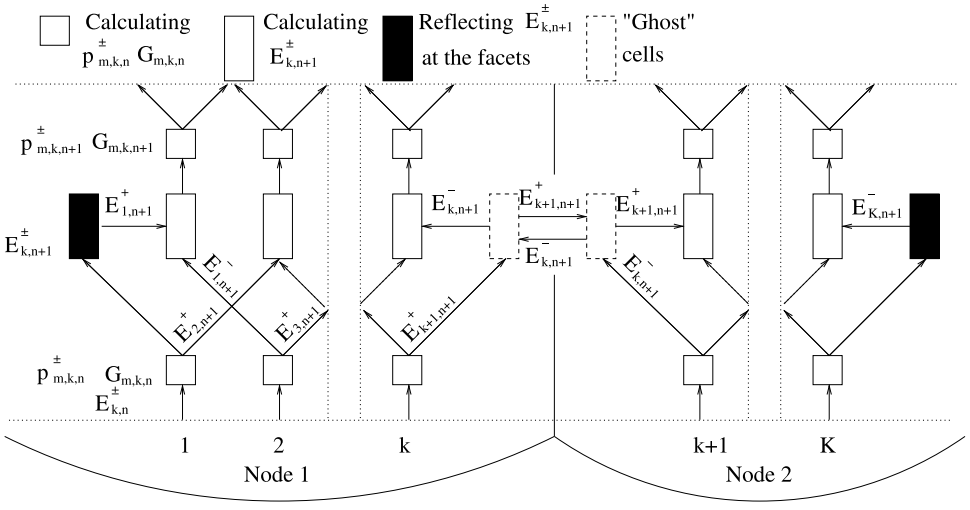

Fig. B.1. Numerical scheme (B.1)–(B.4) with parallelisation realised on two nodes.

References

1. H. Schmeckebier, G. Fiol, C. Meuer, D. Arsenijević, D. Bimberg, Opt. Express **18**, 3415 (2010)
2. D. Bimberg, M. Grundmann, N.N. Ledentsov, *Quantum Dot Heterostructures* (Wiley, 1998)
3. E.U. Rafailov, M.A. Cataluna, W. Sibbett, Nat. Photon. **1**, 395 (2007)
4. M. Grundmann, Physica E **5**, 167 (2000)
5. V.S. Idiatulin, A.V. Uspenskii, Radio Eng. Electron. Phys. **18**, 422 (1973)
6. L.W. Casperson, Phys. Rev. A **21**, 911 (1980)
7. R. Graham, Y. Cho, Opt. Commun. **47**, 52 (1983)
8. L.A. Lugiato, L.M. Narducci, D.K. Bandy, N.B. Abraham, Opt. Commun. **46**, 115 (1983)
9. P. Mandel, Opt. Commun. **44**, 400 (1983)
10. B. Meziane, Opt. Commun. **75**, 287 (1990)
11. B. Meziane, Opt. Commun. **128**, 377 (1996)
12. E. Roldán, G.J. de Valcárcel, F. Silva, J. Opt. Soc. Am. B **18**, 1601 (2001)
13. E. Roldán, G.J. de Valcárcel, Phys. Rev. A **64**, 053805 (2001)
14. F. Prati, E.M. Pessina, G.J. de Valcárcel, E. Roldán, Opt. Commun. **237**, 189 (2003)
15. C. Xing, E.A. Avrutin, J. Appl. Phys. **97**, 104301 (2005)
16. M. Rossetti, P. Bardella, I. Montrosset, IEEE J. Quant. Electron. **47**, 139 (2011)
17. M. Gioannini, P. Bardella, I. Montrosset, IEEE J. Sel. Top. Quant. Electron. **21**, 1 (2015)
18. L.L. Columbo, P. Bardella, I. Montrosset, M. Gioannini, in *2017 International Conference on Numerical Simulation of Optoelectronic Devices (NUSOD)* (2017)
19. L.L. Columbo, P. Bardella, M. Gioannini, Opt. Express **26**, 19044 (2018)
20. E. Cabrera, O.G. Calderón, J.M. Guerra, Phys. Rev. A **70**, 063808 (2004)
21. J. Mukherjee, J.G. McInerney, Phys. Rev. A **79**, 053813 (2009)
22. A.E. Siegman, *Lasers* (University Science Books, Mill Valley, CA, 1986)
23. J. Zehetner, C. Spielmann, E. Krausz, Opt. Lett. **17**, 871 (1992)
24. A.G. Vladimirov, D. Turaev, Radiophys. Quant. Electron. **47**, 857 (2004)
25. A.G. Vladimirov, D. Turaev, G. Kozyreff, Opt. Lett. **29**, 1221 (2004)
26. A.G. Vladimirov, D. Turaev, Phys. Rev. A **72**, 033808 (2005)
27. M. Lichtner, Proc. Am. Math. Soc. **136**, 2091 (2008)
28. A. Pimenov, A.G. Vladimirov, Dynamics of an inhomogeneously broadened passively mode-locked laser. WIAS preprint, 2018
29. A.G. Vladimirov, A.S. Pimenov, D. Rachinskii, IEEE J. Quant. Electr. **45**, 462 (2009)
30. A. Vladimirov, U. Bandelow, G. Fiol, D. Arsenijević, M. Kleinert, D. Bimberg, A. Pimenov, D. Rachinskii, J. Opt. Soc. B **27**, 2102 (2010)
31. U. Bandelow, M. Radziunas, J. Sieber, M. Wolfrum, IEEE J. Quant. Electr. **37**, 183 (2001)
32. J. Javaloyes, S. Balle, Opt. Express **20**, 8496 (2012)
33. E. Viktorov, P. Mandel, A.G.Vladimirov, U. Bandelow, Appl. Phys. Lett. **88**, 201102 (2006)
34. W.E. Lamb Jr, Phys. Rev. **134**, A1429 (1964)
35. K. Engelborghs, T. Luzyanina, G. Samaey, DDE-BIFTOOL v.2.00: A MATLAB package for bifurcation analysis of delay differential equations. Tech. Rep. TW-330, K. U. Leuven, 2001
36. E.A. Avrutin, E.L. Portnoi, Opt. Quant. Electron **40**, 655 (2008)
37. C. Hönninger, R. Paschotta, F. Morier-Genoud, M. Moser, U. Keller, J. Opt. Soc. Am. B **16**, 46 (1999)